AJNR

Dynamic Contrast-Enhanced MR Imaging of Nonenhancing T2 High-Signal-Intensity Lesions in Baseline and Posttreatment Glioblastoma: Temporal Change and Prognostic Value

I. Hwang, S.H. Choi, C.-K. Park, T.M. Kim, S.-H. Park, J.K. Won, I.H. Kim, S.-T. Lee, R.-E. Yoo, K.M. Kang, T.J. Yun, J.-H. Kim and C.-H. Sohn

AJNR Am J Neuroradiol 2020, 41 (1) 49-56
doi: https://doi.org/10.3174/ajnr.A6323
http://www.ajnr.org/content/41/1/49

Dynamic Contrast-Enhanced MR Imaging of Nonenhancing T2 High-Signal-Intensity Lesions in Baseline and Posttreatment Glioblastoma: Temporal Change and Prognostic Value

I. Hwang, S.H. Choi, C.-K. Park, T.M. Kim, S.-H. Park, J.K. Won, I.H. Kim, S.-T. Lee, R.-E. Yoo, K.M. Kang, T.J. Yun, J.-H. Kim, and C.-H. Sohn

ABSTRACT

BACKGROUND AND PURPOSE: The prognostic value of dynamic contrast-enhanced MR imaging on nonenhancing T2 high-signal-intensity lesions in patients with glioblastoma has not been thoroughly elucidated to date. We evaluated the temporal change and prognostic value for progression-free survival of dynamic contrast-enhanced MR imaging–derived pharmacokinetic parameters on nonenhancing T2 high-signal-intensity lesions in patients with glioblastoma before and after standard treatment, including gross total surgical resection.

MATERIALS AND METHODS: This retrospective study included 33 patients who were newly diagnosed with glioblastoma and treated with gross total surgical resection followed by concurrent chemoradiation therapy and adjuvant chemotherapy with temozolomide in a single institution. All patients underwent dynamic contrast-enhanced MR imaging before surgery as a baseline and after completion of maximal surgical resection and concurrent chemoradiation therapy. On the whole nonenhancing T2 high-signal-intensity lesion, dynamic contrast-enhanced MR imaging–derived pharmacokinetic parameters (volume transfer constant [K^{trans}], volume of extravascular extracellular space [v_e], and blood plasma volume [v_p]) were calculated. The Cox proportional hazards regression model analysis was performed to determine the histogram features or percentage changes of pharmacokinetic parameters related to progression-free survival.

RESULTS: Baseline median K^{trans}, baseline first quartile K^{trans}, and posttreatment median K^{trans} were significant independent variables, as determined by univariate analysis ($P < .05$). By multivariate Cox regression analysis including methylation status of O^6-methylguanine-DNA methyltransferase, baseline median K^{trans} was determined to be the significant independent variable and was negatively related to progression-free survival (hazard ratio = 1.48, $P = .003$).

CONCLUSIONS: Baseline median K^{trans} from nonenhancing T2 high-signal-intensity lesions could be a potential prognostic imaging biomarker in patients undergoing gross total surgical resection followed by standard therapy for glioblastoma.

ABBREVIATIONS: CCRT = concurrent chemoradiation therapy; DCE = dynamic contrast-enhanced; K^{trans} = volume transfer constant; MGMT = O^6-methylguanine-DNA methyltransferase; PFS = progression-free survival; TMZ = temozolomide; v_e = volume of extravascular extracellular space; v_p = blood plasma volume

The standard treatment of glioblastoma is a multimodality strategy including maximal safe surgical resection and radiation therapy with concomitant and adjuvant temozolomide (TMZ).[1,2] Glioblastoma is a diffusely infiltrating and widespread malignant neoplasm. The main target for surgical resection to improve survival is a contrast-enhancing, high-grade portion of the tumor with a leaky BBB.[3,4] However, certain nonenhancing infiltrative tumor cells may remain after surgical resection and

Received July 1, 2019; accepted after revision October 2.

From the Department of Radiology (I.H., S.H.C., R.-E.Y., K.M.K., T.J.Y., J.-H.K., C.-H.S.), Center for Nanoparticle Research; Institute for Basic Science, and School of Chemical and Biological Engineering (S.H.C.); Department of Neurosurgery and Biomedical Research Institute (P.C.-K.); Department of Internal Medicine and Cancer Research Institute (T.M.K.); Department of Pathology (S.-H.P., J.K.W.), Department of Radiation Oncology and Cancer Research Institute (I.H.K.); and Department of Neurology (S.-T.L.), Seoul National University Hospital, Seoul, Korea.

This study was supported by grants from the Korea Healthcare Technology R&D Projects, Ministry for Health, Welfare & Family Affairs (HI16C1111); the Brain Research Program through the National Research Foundation of Korea funded by the Ministry of Science, ICT & Future Planning (2016M3C7A1914002); the Basic Science Research Program through the National Research Foundation of Korea funded by the Ministry of Science, ICT & Future Planning (2017R1A2B2006526); the Creative-Pioneering Researchers Program through Seoul National University, and Project Code (IBS-R006-D1).

Please address correspondence to Seung Hong Choi, MD, PhD, Department of Radiology, Seoul National University Hospital, 101 Daehak-ro, Jongno-gu, Seoul, 03080, Korea; e-mail: verocay@snuh.org

Indicates open access to non-subscribers at www.ajnr.org
Indicates article with supplemental on-line table.
Indicates article with supplemental on-line photo.
http://dx.doi.org/10.3174/ajnr.A6323

intermingle with peritumoral edema. Unfortunately, those lesions are difficult to distinguish because they are similarly presenting as high-signal-intensity lesions on T2-weighted or FLAIR images. The biologic nature of nonenhancing T2 high-signal-intensity lesions could be more important for the prognosis than that of the contrast-enhancing high-grade tumor portion, which would be removed by maximal safe surgical resection.

Dynamic contrast-enhanced (DCE) MR imaging could provide information on permeability and angiogenesis by quantitative pharmacokinetic parameters.[5,6] Previous studies with DCE-MR imaging in gliomas have already demonstrated the capability of predicting histologic grading, differentiating pseudoprogression from progression, and predicting the progression of persistent enhancing nodules after standard treatment.[7-9] A recent histopathologic study suggested that nonenhancing tumor contains a comparable amount of infiltrative tumor to enhancing tumor in glioblastomas.[10] We hypothesized that a variable proportion of peritumoral edema, low-grade infiltrative tumor, or even nonenhancing high-grade tumors might coexist in the nonenhancing T2 high-signal-intensity lesions. As the tumor grade increases, it tends to have a large portion of immature vasculature. Therefore, DCE-MR imaging–derived pharmacokinetic parameters might have the potential to predict the biologic behavior of those lesions. Meanwhile, the permeability of the BBB may affect the delivery of the chemotherapeutic drug to brain tissue. Although brain tumors are different from other tumors due to their unique BBB structure, previous studies of malignant tumors outside the brain, such as cervical cancer, colorectal cancer, and lung cancer, have demonstrated that increased permeability or angiogenesis was related to a favorable tumor response.[11-13] Therefore, there is a possibility that increased permeability at certain time points might be related to a favorable treatment response.

Some studies have focused on the perfusion characteristics of nonenhancing T2 high-signal-intensity lesions in glioblastoma to predict prognosis.[14-16] However, there have been few investigations of the DCE-MR imaging–derived pharmacokinetic parameters of nonenhancing T2 high-signal-intensity lesions of glioblastoma at the time of baseline and post concurrent chemoradiation therapy (CCRT) and their temporal change.

Therefore, the purpose of this study was to evaluate the temporal change and prognostic value for progression-free survival (PFS) of DCE-MR imaging–derived pharmacokinetic parameters on nonenhancing T2 high-signal-intensity lesions in patients with glioblastoma before and after standard treatment, including gross total surgical resection.

MATERIALS AND METHODS

Study Population

The institutional review board of our institution approved this single-center, retrospective study, and informed consent was waived. By means of a data base search between January 2010 and December 2017, two hundred eighty-nine consecutive patients were confirmed to have glioblastoma by histopathologic diagnosis. Two neuropathologists performed the histopathologic diagnosis at our institution (S.-H.P. and J.K.W. with 32 and 17 years of experience in pathology, respectively). Among the patients, the eligible study population was defined by the following inclusion criteria: The patient had a histopathologic diagnosis of supratentorial glioblastoma, underwent baseline DCE-MR imaging 24–48 hours before the operation, underwent maximal surgical resection (near-total or gross-total resection) followed by CCRT with TMZ administration, and underwent posttreatment DCE-MR imaging within 1 month after completion of CCRT. Ultimately, 33 patients met the inclusion criteria and were included in our study (Fig 1). All patients except 2 had 6 cycles of adjuvant TMZ administration 1 month after the completion of CCRT. One patient stopped adjuvant TMZ after 4 cycles because of disease progression and switched to second-line chemotherapy; another patient was discontinued after 2 cycles of TMZ administration due to severe skin eruption.

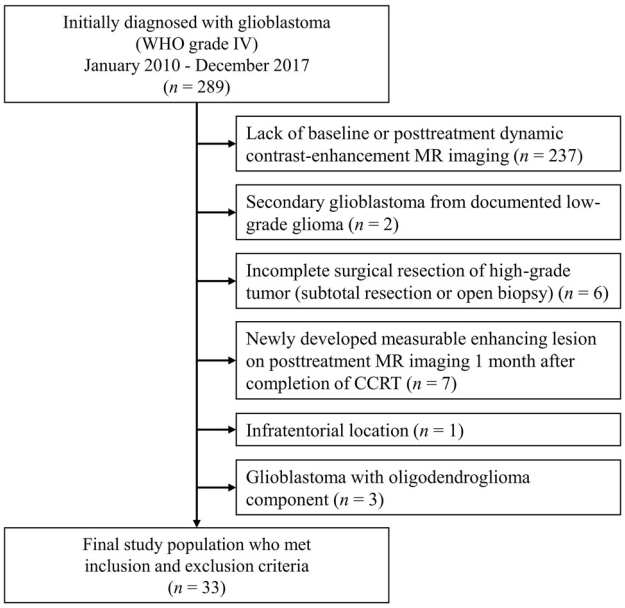

FIG 1. Flow chart for patient selection.

Calculation of PFS Time

All patients routinely visited the outpatient clinic and underwent follow-up brain MR imaging with a brain tumor evaluation protocol at our institution every 3 months for the first 2 years. Then the follow-up period was extended to 6 months if the patient had no clinical or radiologic evidence of progression. Clinicians and radiologists assessed the patient's response to treatment using the Response Assessment in Neuro-Oncology criteria.[17] If the patient met at least 1 of the following criteria at each visit, the patient was diagnosed with disease progression: 1) >25% increase in the sum of the products of the perpendicular diameters of enhancing lesions, compared with the smallest tumor measurement obtained either at baseline or best response; 2) substantial increase in T2/FLAIR nonenhancing lesion; 3) any new lesion; 4) evident clinical deterioration not attributable to other causes apart from the tumor; and 5) clear progression of nonmeasurable disease. If there was imaging evidence of an increasingly enhancing lesion that did not meet the criteria of progression, short-term follow-up imaging was performed in 1–2 months. Then, the progression of disease was confirmed by subsequent

imaging or by histopathologic diagnosis. In case of changing the treatment plan due to disease progression, as decided by the multidisciplinary clinic in our institution, it was also regarded as a disease progression. The PFS was calculated between the date of initial imaging diagnosis and the date assessed as disease progression or the last follow-up date if the patient had no evidence of disease at the last follow-up visit.

Image Acquisition

All patients underwent brain MR imaging using a 3T MR imaging scanner (Magnetom Verio or Skyra; Siemens, Erlangen, Germany) with a 32-channel head coil. Our institution's routine brain MR imaging protocol for brain tumor evaluation included pre- and postcontrast 3D T1-weighted MPRAGE sequences (TR, 558 ms; TE, 1.9 ms; flip angle, 9°; matrix, 256 × 232; FOV, 220 × 250 mm; section thickness, 1 mm; and NEX, 1), a transverse T2 FLAIR sequence (TR, 9000 ms; TE, 97; ms; TI, 2500 ms; flip angle, 130°; matrix, 384 × 348; FOV, 199 × 220 mm; section thickness, 5 mm; and NEX, 1), and transverse T2WI with a TSE sequence (TR, 5160 ms; TE, 91 ms; flip angle, 124°–130°; matrix, 640 × 510–580; FOV, 175–199 × 220 mm; section thickness, 5 mm; NEX, 1).

DCE-MR images were obtained using a transverse T1-weighted spoiled gradient-echo sequence (TR, 2.8 ms; TE, 1.0 ms; flip angle, 10°; matrix, 192 × 192; FOV, 240 × 240; and section thickness, 3 mm) after intravenous administration of gadobutrol (Gadovist; Bayer Schering Pharma, Berlin, Germany) at a dose of 0.1 mmol/kg of body weight and at a rate of 4 mL/s followed by a 30-mL saline chaser using a power injector (Spectris; MedRad, Indianola, Pennsylvania). Sixty dynamic scans with a time resolution of 4.97 seconds were acquired with 40 slices of transverse plane images; the total acquisition time was 5 minutes 8 seconds.

Image Analysis

DCE-MR images were transferred to dedicated workstations, and postprocessing was performed with commercial software (nordicICE 4.0.6; NordicNeuroLab, Bergen, Norway).

We performed coregistration of FLAIR and DCE-MR imaging on postcontrast 3D T1WI as structural imaging achieved automatically by an algorithm that found an optimal rigid transformation based on the geometric information.[18] If there was geometric distortion due to postsurgical changes, manual correction was performed for the best match of nonenhancing T2 high-signal-intensity lesions. After the motion correction of DCE-MR imaging volume, deconvolution with the arterial input function was performed in the pharmacokinetic model. After the ROI was positioned in the superior sagittal sinus at the level of the lateral ventricles, the average arterial input function curve from 3 to 5 pixels of the best arterial input function candidate was semiautomatically determined. The baseline T1 value was fixed at 1000 ms in this study because it would give more reliable results.[19,20] Subsequently, DCE-MR imaging–derived pharmacokinetic parametric maps were generated by the extended Tofts model[21]; volume transfer constant map (K^{trans}, minute^{-1}), extravascular extracellular space per unit volume of tissue map (v_e, percentage), and blood plasma volume per unit volume of tissue map (v_p, percentage) were calculated on a pixel-by-pixel basis.

Two investigators (I.H. and S.H.C., with 8 and 17 years of experience in neuroradiology) carefully determined the VOI by consensus in every section of nonenhancing T2 high-signal-intensity lesions on FLAIR images. Enhancing areas on the postcontrast T1-weighted images and cystic/necrotic areas or macrovessels were carefully avoided. The pharmacokinetic parameters on K^{trans}, v_e, and v_p maps were measured at baseline and on the posttreatment study. The On-line Figure illustrates the representative image-analysis process. For further quantitative analysis, we performed histogram analysis from the total voxel values; the mean, SD, skewness, kurtosis, median, first and third quartile values, fifth and 95th percentile values of each pharmacokinetic parameter, as well as the mask volume of VOIs were calculated. We included the voxels in which each DCE pharmacokinetic parameter value was >0. Furthermore, the percentage change between posttreatment and baseline values of each pharmacokinetic parameter was calculated in each subject as follows:

Percentage Change = (Posttreatment – Baseline)/Baseline × 100.

Other Clinical and Genetic Parameters

In addition to demographic characteristics, the Karnofsky Performance Status score before the operation and the radiation dose of CCRT were investigated to evaluate the prognostic value. Furthermore, the following genetic alterations were investigated in this study: mutation of *isocitrate dehydrogenase* (*IDH*) and promoter methylation of O^6-methylguanine-DNA methyltransferase (MGMT).

Statistical Analysis

All statistical analyses were performed by open-source statistical language (R for Windows, Version 3.5.1) with the survival analysis package (survival).[22] In all statistical tests, a P value < .05 was considered a significance level. Descriptive statistics summarized clinical and genetic characteristics. A univariate Cox proportional hazards regression model was used to investigate differentiating clinical, genetic, and pharmacokinetic parameters for PFS. A variance inflation factor was calculated for the significant pharmacokinetic parameters by univariate analysis, and variables with >10 were sequentially excluded to exclude variables having multicollinearity. Finally, multivariate Cox proportional hazard model analyses were performed to identify independent pharmacokinetic parameters for differentiating PFS. The optimal cutoff value was calculated by the published method using the R language.[23] After that step, the Kaplan-Meier survival curve was plotted, and the log-rank test was performed.

RESULTS

Clinical and Genetic Characteristics

Clinical and genetic characteristics are summarized in Table 1. The median PFS of our study population was 22.6 months (689 days). Twenty-six patients were diagnosed with tumor progression during the follow-up period. The prevalence of an *IDH* mutation was 6.1%, and the promoter methylation of MGMT was 66.7% (Table 1).

The patients with promoter methylation of MGMT of the tumor showed significantly better survival with a hazard ratio of 0.256 (P = .001). Otherwise, none of the clinical or genetic

Table 1: Clinical and genetic characteristics of our study population and prognostic value by univariate Cox regression test

	Mean (SD) or No. (%)	Hazard Ratio (95% CI)	*P* Value
Age (years)	55.5 (13.4)	1.02 (0.990–1.06)	.172
Sex			
Men	21 (63.6%)	0.887 (0.393–2.00)	.772
Women	12 (36.4%)		
Radiation dose			
Hypofractionated (45 Gy in 15 fractions)	6 (18.2%)	1.51 (0.593–3.84)	.388
Conventional long course (>60 Gy)	27 (81.8%)		
Karnofsky Performance Status score			
<70	3 (9.1%)	0.820 (0.193–3.50)	.789
≥70	30 (90.9%)		
IDH1 or *2* mutation			
Present	2 (6.1%)	0.324 (0.0432–2.436)	.274
Absent	31 (93.9%)		
MGMT promoter methylation			
Methylated	22 (66.7%)	0.256 (0.113–0.577)	.001
Unmethylated	11 (33.3%)		
Baseline T2 high-signal-intensity volume (mL)	59.5 (29.0)	0.996 (0.982–1.01)	.573
Posttreatment T2 high-signal-intensity volume (mL)	16.6 (24.8)	0.996 (0.978–1.01)	.668
Percentage change T2 high-signal-intensity volume	−64.3% (44.8%)	1.04 (0.412–2.63)	.934

Table 2: Significant variables by univariate Cox proportional hazards model analysis of pharmacokinetic parameters

	Hazard Ratio (95% CI)[a]	*P* Value
Baseline first quartile K^{trans}	1.51 (1.08–2.12)	.016
Baseline median K^{trans}	1.26 (1.01–1.57)	.038
Posttreatment median K^{trans}	1.22 (1.03–1.45)	.024

[a] Hazard ratios for K^{trans} are adjusted for a unit change of 0.001 min^{-1}.

characteristics, the volume of VOI, or its percentage change showed statistical significance by univariate Cox regression (Table 1).

Univariate Cox Proportional Hazards Regression Model for DCE-MR Imaging–Derived Pharmacokinetic Parameters

The univariate Cox regression model of each histogram feature of DCE-MR imaging–derived pharmacokinetic parameters from baseline and posttreatment T2 high-signal-intensity lesions was performed and is described in the On-line Table. The variables with *P* values < .05 by the Wald test were baseline median K^{trans}, baseline first quartile K^{trans}, and posttreatment median K^{trans} (Table 2). Although the percentage change of kurtosis K^{trans} was marginally insignificant (*P* = .066), the percentage change of the pharmacokinetic parameter was not determined to be a significant variable.

Multivariate Cox Proportional Hazards Regression Model for DCE-MR Imaging–Derived Pharmacokinetic Parameters

Both the baseline median and first quartile K^{trans} showed significance on univariate analysis. We selected the median value, rather than the first quartile, for further analysis because of the better interpretability of this parameter. After that step, we performed a multivariate Cox regression test with baseline and posttreatment median K^{trans}. The Cox regression model with both baseline and posttreatment median K^{trans} showed that neither variable was significant (Table 3). However, after adding the methylation status of MGMT as a clinical variable in the model, the multivariate Cox regression test revealed that the baseline median K^{trans} and the methylation status of MGMT were significant independent variables (Table 3). Finally, we performed a multivariate Cox regression test with a stepwise variable selection method including these variables: baseline median K^{trans}, posttreatment median K^{trans}, percentage change of kurtosis K^{trans}, and the methylation status of MGMT. The stepwise method selected the variables of baseline median K^{trans} and the methylation status of MGMT as significant independent variables (*P* = .003 and *P* < .001, respectively). The percentage change of kurtosis K^{trans} was included in the model, but it was not a significant variable (*P* = .108). The posttreatment median K^{trans} was excluded from the model by stepwise variable selection.

Comparison of Survival Curves by the Binary Representation of Differentiating Variables

Kaplan-Meier survival plots were compared by the binary representation of the baseline median K^{trans} (Fig 2). The calculated optimal cutoff value for baseline median K^{trans} was 0.00470 min^{-1}. By means of the log-rank test, baseline median K^{trans} from T2 high-signal-intensity lesions showed a significant difference in the survival curve (*P* = .030). In subgroup analysis grouped by the methylation status of MGMT, the significant difference of the survival curve by baseline median K^{trans} was seen only in patients with MGMT methylated (*n* = 22, *P* = .029), while it did not reach statistical significance in patients with unmethylated MGMT (*n* = 11, *P* = .256). However, the survival curves showed the consistent trend of the higher value group of baseline median K^{trans} being related to poor survival. Representative cases are illustrated in Fig 3.

DISCUSSION

Our results demonstrate that increased baseline median K^{trans} from nonenhancing T2 high-signal-intensity lesions was associated with poor survival by multivariate Cox regression analysis. However, there was no statistically significant pharmacokinetic parameter from the posttreatment study or its percentage change between baseline and posttreatment.

Our study intended to evaluate nonenhancing T2 high-signal-intensity lesions of glioblastoma. These lesions have been regarded as a mixture of peritumoral edema and infiltrative tumor cells, even including postsurgical changes and radiation effects after treatment. However, in cases in which a sufficient extent of tumor resection was achieved, some patients eventually had tumor recurrence from the near-resection margin.[24] Therefore, we postulated that the character of the remaining nonenhancing T2 high-signal-intensity lesions would be more critical to predict patient survival in cases of gross total resection. A few studies have investigated DCE-MR imaging-derived pharmacokinetic parameters for the prognostic value of T2 high-signal-intensity lesions in high-grade gliomas. Jensen et al[25] revealed, from a small study group, that a higher v_e value of peritumoral edema was associated with favorable overall survival. A recent prospective study extensively investigated perfusion characteristics at multiple time points, including baseline, during CCRT with TMZ, and during 6 cycles of adjuvant TMZ.[26] Their results supported the higher K^{trans} of enhancing tumors at the fifth week during CCRT being associated with worse PFS, though baseline relative CBV and CBF in the edema region were marginally statistically insignificant.

In contrast to previous studies, our study evaluated the prognostic value of baseline and posttreatment, in particular post-CCRT DCE-MR imaging-derived pharmacokinetic parameters and their temporal changes with histogram analysis. In addition, our study included patients who underwent gross surgical resection and had no remaining measurable enhancing lesions on follow-up MR imaging. Therefore, the study population was more homogeneous than previous studies, and we could evaluate the true nature of T2 high-signal-intensity lesions at the posttreatment period. Our results were consistent with the findings of a previous study by Kim et al,[16] agreeing that baseline K^{trans} of T2 high-signal-intensity lesions has potential prognostic value. K^{trans} is the most representative marker of permeability in the DCE-MR imaging parameter.[27] K^{trans} has been reported to be able to predict the grade of glioma because aggressive tumor cells exhibit a higher portion of immature vessels, resulting in leaky vasculature.[7] Therefore, a higher baseline K^{trans} value might reflect the aggressiveness of infiltrating tumor cells in nonenhancing T2 high-signal-intensity lesions and is probably related to worse PFS.

Unfortunately, our study did not obtain a statistically significant prognostic value of posttreatment DCE-MR imaging–derived pharmacokinetic parameters and their temporal change. The median K^{trans} from nonenhancing T2 high-signal-intensity lesions in the posttreatment study showed significance by univariate analysis. However, multivariate analysis revealed that it was not statistically significant for PFS. According to a published study, the

Table 3: Multivariate Cox proportional hazard model analysis of pharmacokinetic parameters[a]

	Hazard Ratio (95% CI)[a]	*P*-value
Model 1: without MGMT methylation status		
Baseline median K^{trans}	1.19 (0.934–1.52)	.158
Posttreatment median K^{trans}	1.16 (0.958–1.40)	.129
Model 2: with MGMT methylation status		
Baseline median K^{trans}	1.48 (1.12–1.93)	.005
Posttreatment median K^{trans}	1.01 (0.840–1.21)	.935
Presence of MGMT methylation	0.150 (0.0541–0.417)	<.001
Model 3: by stepwise variable selection[b]		
Baseline median K^{trans}	1.49 (1.15–1.92)	.003
Posttreatment median K^{trans}		
Percentage change of kurtosis K^{trans}	1.26 (0.951–1.66)	.108
Presence of MGMT methylation	0.143 (0.0541–0.375)	<.001

[a] Hazard ratios for K^{trans} were adjusted for a unit change of 0.001 min^{-1}.
[b] A stepwise variable selection including baseline median K^{trans}, posttreatment median K^{trans}, the percentage change of kurtosis K^{trans}, and the methylation status of MGMT.

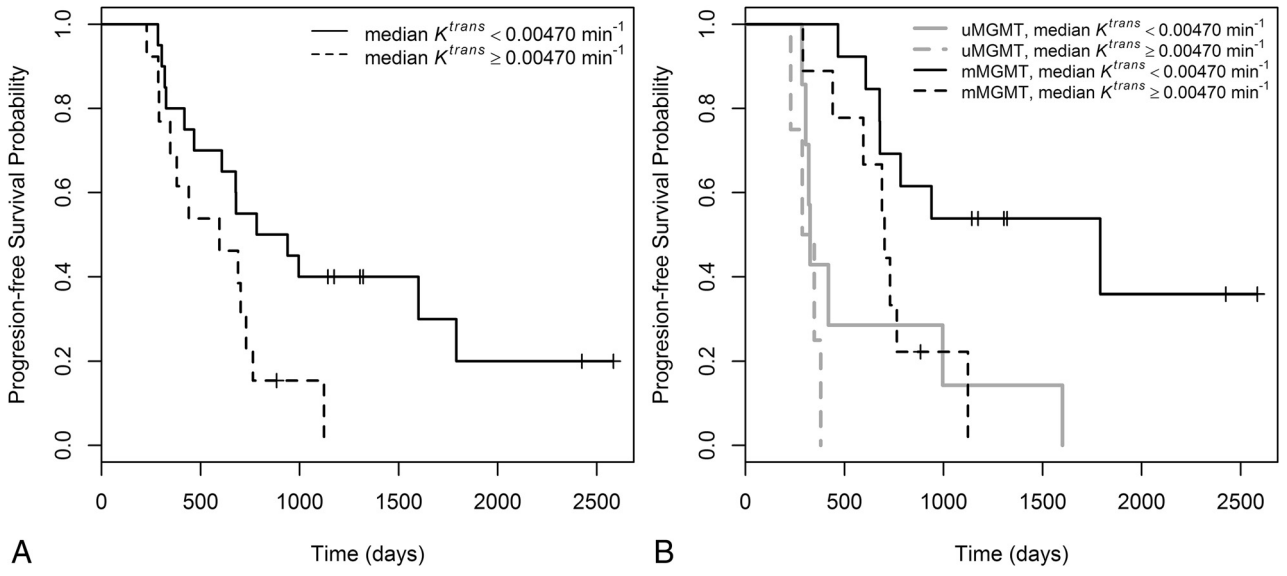

FIG 2. Kaplan-Meier curves of baseline median K^{trans} from a T2 high-signal-intensity lesion (*A*) and subgroup curves grouped by the methylation status of MGMT (*B*). mMGMT indicates methylated O^6-methylguanine-DNA methyltransferase; uMGMT, unmethylated MGMT.

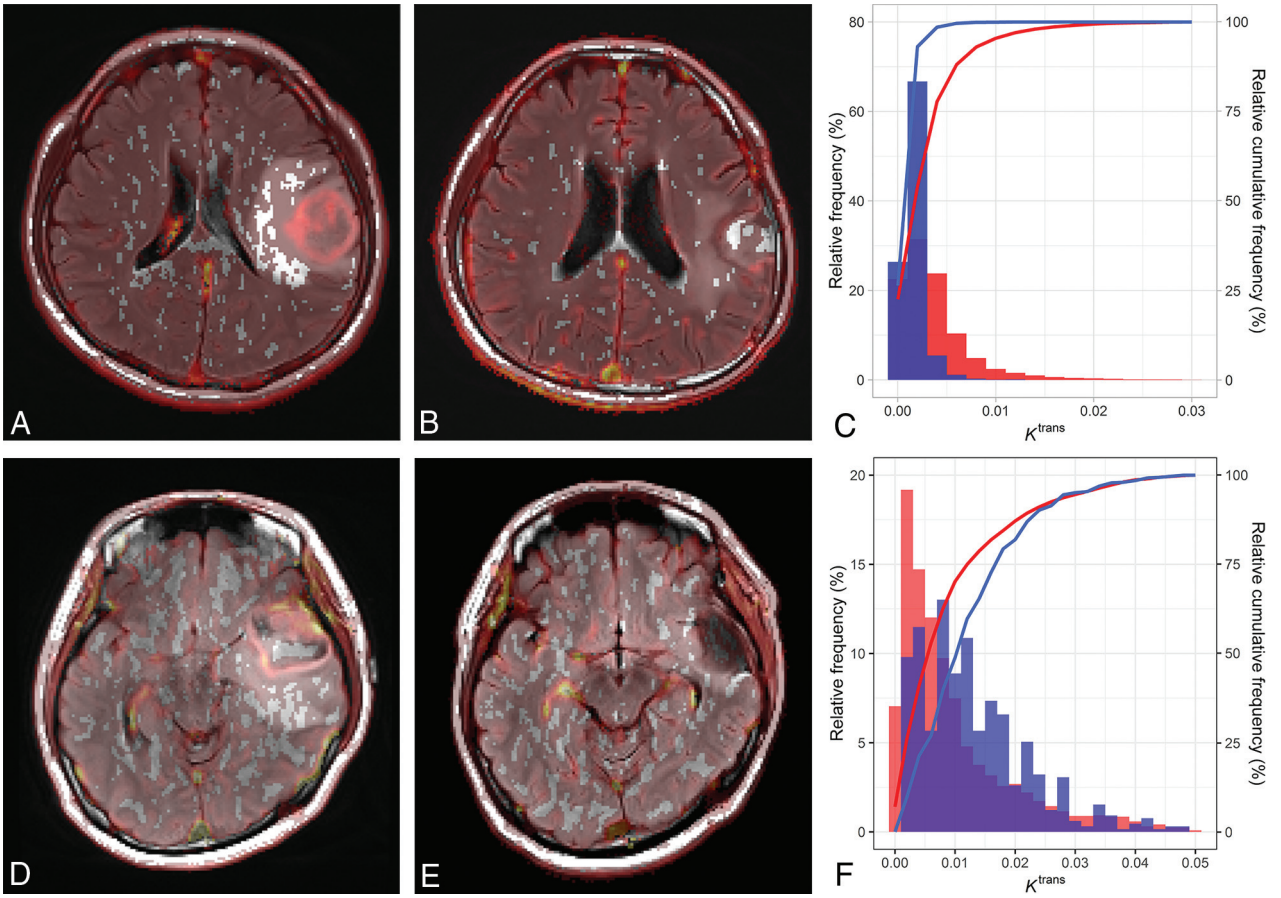

FIG 3. Representative cases. A 54-year-old man who was diagnosed with glioblastoma *IDH* wild-type in the left frontal lobe. Nonenhancing T2 high-signal-intensity lesions around the enhancing mass (postcontrast images are not shown) are noted on baseline FLAIR images with an overlay of the K^{trans} map (*A*). Posttreatment FLAIR images with an overlay K^{trans} map show residual T2 high-signal-intensity lesions around the surgical margin (*B*). A cumulative histogram is shown in *C*. The *red bar* and *line* indicate the distribution of the baseline K^{trans} of nonenhancing T2 high-signal-intensity lesions, while the *blue bar* and *line* show the distribution of the posttreatment K^{trans} values. The baseline median K^{trans} of nonenhancing T2 high-signal-intensity lesions was 0.00258 min^{-1}. The patient survived 1600 days after the diagnosis without progression. A 42-year-old woman was diagnosed with glioblastoma *IDH* wild-type in the left temporal lobe. Baseline (*D*) and posttreatment (*E*) FLAIR images with an overlay of the K^{trans} map show T2 high-signal-intensity lesions around the enhancing tumor (postcontrast images are not shown), partially removed by an operation, but remnant T2 high-signal-intensity lesions are noted. A cumulative histogram is shown in *F*. The baseline median K^{trans} is 0.00670 min^{-1}. The progression-free survival was 347 days, and the recurrent enhancing tumor developed along the superior-posterior surgical margin on subsequent follow-up MR imaging.

initial increase and subsequent overall decrease of K^{trans} of enhancing tumors were observed in nonresponders during CCRT in glioblastoma.[28] The study by these researchers also did not find prognostic value by multivariate Cox regression analysis, except for interval change of K^{trans} between the pre- and midtreatment scanning during CCRT. A possible explanation of our finding is that the subsequent change in DCE parameters after CCRT could reduce differences between better and worse PFS groups. In addition, some areas of nonenhancing T2 high-signal-intensity lesions were removed by an operation, and the nature of nonenhancing T2 high-signal-intensity lesions might not be the same between baseline and posttreatment examinations.

Most interesting, the prognostic value of baseline K^{trans} of nonenhancing T2 high-signal-intensity lesions was independent of the methylation status of the MGMT promoter. Methylation of the MGMT promoter is associated with favorable survival for patients with glioblastoma who are treated with CCRT with TMZ.[29] The baseline DCE-MR imaging–derived pharmacokinetic parameters may reflect a different aspect of tumor biology than the methylation status of the MGMT promoter. In contrast, the posttreatment K^{trans} was not significant after adding the methylation status of the MGMT promoter. There is a possibility that the posttreatment K^{trans} has a relationship to the methylation status of the MGMT promoter. However, that would be beyond the scope of our study, and further studies are warranted.

In our study, only voxels with values greater than zero in the DCE parameter map were used for further histogram analysis. A previous study[28] used the DCE parameter >0 as the criterion of successfully fitted pixels. However, our study measured nonenhancing T2 high-signal-intensity lesions. In the edema portion where the BBB is intact, the K^{trans} would be near zero. By means of DCE curve fitting, a particular part of those areas would yield zero or even negative K^{trans} values; therefore, it would not necessarily be a fitting failure. Although particular voxels affected by motion artifacts also yielded nonphysiologic K^{trans} values due to

fitting failure, we believe that such a portion would not be substantial because we performed motion correction. However, we performed analysis with the positive DCE parameter voxel value for the comparability with previous studies and to maintain physiologic meaning.

The present study had a few limitations. First, the retrospective study design had potential selection bias. To minimize the selection bias, we attempted to include all consecutive patients diagnosed with glioblastoma and meeting the inclusion criteria. Second, we used 2D-FLAIR images to draw VOI masks. Therefore, there was a potential risk of spatial mismatch between FLAIR-based VOIs and DCE parametric maps due to the partial volume effect, though we coregistered image volumes. Furthermore, due to the intrinsic infiltrative nature of tumors, the margin of T2 high-signal-intensity lesions did not have a clear border, which may limit the reproducibility of determining the margin of the lesion on FLAIR images. Acquisition of the 3D-FLAIR images and use of automatic or semiautomatic segmentation techniques may improve reproducibility for the lesion. Third, a small sample size limits our ability to derive generalized conclusions from our results. However, to evaluate the nature of nonenhancing T2 high-signal-intensity lesions after the gross total resection of enhancing tumors, we had to exclude a large number of patients who had remnant measurable enhancing tumors immediately after surgical resection. Therefore, there is a limitation to generalizing our results to all patients with glioblastoma. Moreover, our study excluded subjects who demonstrated measurable enhancing lesions in the posttreatment study. For that reason, we could not evaluate pseudoprogression, which shows newly developed enhancing lesions during CCRT, but it might be related to favorable survival, though this is still controversial.[30,31] In addition, our results showed no statistical survival difference by the presence of the *IDH* mutation. It was possibly due to a small number of patients with *IDH* mutation with glioblastoma in our study population, which had insufficient statistical power. Finally, we investigated only PFS, not overall survival. However, the PFS is known to be a surrogate marker of overall survival in glioblastoma.[32]

CONCLUSIONS

Baseline median K^{trans} from nonenhancing T2 high-signal-intensity lesions could be a potential prognostic imaging biomarker in patients undergoing gross total surgical resection followed by standard therapy for glioblastoma. Our results suggest that DCE pharmacokinetic parameters derived from baseline nonenhancing T2 high-signal-intensity lesions have prognostic value; in contrast, those derived during the posttreatment period or percentage change values appear to have little prognostic value.

Disclosures: Seung Hong Choi—*RELATED*: *Grant*: government fund.* Tae Min Kim—*UNRELATED*: *Grants/Grants Pending*: AstraZeneca–Korea Health Industry Development Institute. *Money paid to the institution.

REFERENCES

1. Stupp R, Mason WP, van den Bent MJ, et al. **Radiotherapy plus concomitant and adjuvant temozolomide for glioblastoma.** *N Engl J Med* 2005;352:987–96 CrossRef Medline
2. Stupp R, Hegi ME, Mason WP, et al; European Organisation for Research and Treatment of Cancer Brain Tumour and Radiation Oncology Groups; National Cancer Institute of Canada Clinical Trials Group. **Effects of radiotherapy with concomitant and adjuvant temozolomide versus radiotherapy alone on survival in glioblastoma in a randomised phase III study: 5-year analysis of the EORTC-NCIC trial.** *Lancet Oncol* 2009;10:459–66 CrossRef Medline
3. Tate MC, Aghi MK. **Biology of angiogenesis and invasion in glioma.** *Neurotherapeutics* 2009;6:447–57 CrossRef Medline
4. Smets T, Lawson TM, Grandin C, et al. **Immediate post-operative MRI suggestive of the site and timing of glioblastoma recurrence after gross total resection: a retrospective longitudinal preliminary study.** *Eur Radiol* 2013;23:1467–77 CrossRef Medline
5. Tofts PS, Brix G, Buckley DL, et al. **Estimating kinetic parameters from dynamic contrast-enhanced T(1)-weighted MRI of a diffusible tracer: standardized quantities and symbols.** *J Magn Reson Imaging* 1999;10:223–32 CrossRef Medline
6. Harrer JU, Parker GJ, Haroon HA, et al. **Comparative study of methods for determining vascular permeability and blood volume in human gliomas.** *J Magn Reson Imaging* 2004;20:748–57 CrossRef Medline
7. Jung SC, Yeom JA, Kim JH, et al. **Glioma: application of histogram analysis of pharmacokinetic parameters from T1-weighted dynamic contrast-enhanced MR imaging to tumor grading.** *AJNR Am J Neuroradiol* 2014;35:1103–10 CrossRef Medline
8. Yun TJ, Park CK, Kim TM, et al. **Glioblastoma treated with concurrent radiation therapy and temozolomide chemotherapy: differentiation of true progression from pseudoprogression with quantitative dynamic contrast-enhanced MR imaging.** *Radiology* 2015;274:830–40 CrossRef Medline
9. Yoo RE, Choi SH, Kim TM, et al. **Dynamic contrast-enhanced MR imaging in predicting progression of enhancing lesions persisting after standard treatment in patients with glioblastoma: a prospective study.** *Eur Radiol* 2017;27:3156–66 CrossRef Medline
10. Eidel O, Burth S, Neumann JO, et al. **Tumor infiltration in enhancing and non-enhancing parts of glioblastoma: a correlation with histopathology.** *PLoS One* 2017;12:e0169292 CrossRef Medline
11. Zahra MA, Tan LT, Priest AN, et al. **Semiquantitative and quantitative dynamic contrast-enhanced magnetic resonance imaging measurements predict radiation response in cervix cancer.** *Int J Radiat Oncol Biol Phys* 2009;74:766–73 CrossRef Medline
12. Kim H, Hartman YE, Zhai G, et al. **Dynamic contrast-enhanced MRI evaluates the early response of human head and neck tumor xenografts following anti-EMMPRIN therapy with cisplatin or irradiation.** *J Magn Reson Imaging* 2015;42:936–45 CrossRef Medline
13. Tao X, Wang L, Hui Z, et al. **DCE-MRI perfusion and permeability parameters as predictors of tumor response to CCRT in patients with locally advanced NSCLC.** *Sci Rep* 2016;6:35569 CrossRef Medline
14. Artzi M, Bokstein F, Blumenthal DT, et al. **Differentiation between vasogenic-edema versus tumor-infiltrative area in patients with glioblastoma during bevacizumab therapy: a longitudinal MRI study.** *Eur J Radiol* 2014;83:1250–56 CrossRef Medline
15. Bag AK, Cezayirli PC, Davenport JJ, et al. **Survival analysis in patients with newly diagnosed primary glioblastoma multiforme using pre- and post-treatment peritumoral perfusion imaging parameters.** *J Neurooncol* 2014;120:361–70 CrossRef Medline
16. Kim R, Choi SH, Yun TJ, et al. **Prognosis prediction of nonenhancing T2 high signal intensity lesions in patients with glioblastoma after standard treatment: application of dynamic contrast-enhanced MR imaging.** *Eur Radiol* 2017;27:1176–85 CrossRef Medline
17. Wen PY, Macdonald DR, Reardon DA, et al. **Updated response assessment criteria for high-grade gliomas: response assessment in neuro-oncology working group.** *J Clin Oncol* 2010;28:1963–72 CrossRef Medline
18. Pluim JP, Maintz JB, Viergever MA. **Mutual-information-based registration of medical images: a survey.** *IEEE Trans Med Imaging* 2003;22:986–1004 CrossRef Medline

19. Haacke EM, Filleti CL, Gattu R, et al. **New algorithm for quantifying vascular changes in dynamic contrast-enhanced MRI independent of absolute T1 values.** *Magn Reson Med* 2007;58:463–72 CrossRef Medline
20. Nam JG, Kang KM, Choi SH, et al. **Comparison between the prebolus T1 measurement and the fixed T1 value in dynamic contrast-enhanced MR imaging for the differentiation of true progression from pseudoprogression in glioblastoma treated with concurrent radiation therapy and temozolomide chemotherapy.** *AJNR Am J Neuroradiol* 2017;38:2243–50 CrossRef Medline
21. Tofts PS, Kermode AG. **Measurement of the blood-brain-barrier permeability and leakage space using dynamic MR imaging, I: fundamental-concepts.** *Magn Reson Med* 1991;17:357–67 CrossRef Medline
22. R Core Team. **R: A Language and Environment for Statistical Computing.** https://www.r-project.org/. Accessed May 4, 2019
23. Chang C, Hsieh MK, Chang WY, et al. **Determining the optimal number and location of cutoff points with application to data of cervical cancer.** *PLoS One* 2017;12:e0176231 CrossRef Medline
24. Gaspar LE, Fisher BJ, Macdonald DR, et al. **Supratentorial malignant glioma: patterns of recurrence and implications for external beam local treatment.** *Int J Radiat Oncol Biol Phys* 1992;24:55–57 CrossRef Medline
25. Jensen RL, Mumert ML, Gillespie DL, et al. **Preoperative dynamic contrast-enhanced MRI correlates with molecular markers of hypoxia and vascularity in specific areas of intratumoral microenvironment and is predictive of patient outcome.** *Neuro Oncol* 2014;16:280–91 CrossRef Medline
26. Ly KI, Vakulenko-Lagun B, Emblem KE, et al. **Probing tumor microenvironment in patients with newly diagnosed glioblastoma during chemoradiation and adjuvant temozolomide with functional MRI.** *Sci Rep* 2018;8:17062 CrossRef Medline
27. Koh TS, Bisdas S, Koh DM, et al. **Fundamentals of tracer kinetics for dynamic contrast-enhanced MRI.** *J Magn Reson Imaging* 2011;34:1262–76 CrossRef Medline
28. Bisdas S, Smrdel U, Bajrovic FF, et al. **Assessment of progression-free-survival in glioblastomas by intratreatment dynamic contrast-enhanced MRI.** *Clin Neuroradiol* 2016;26:39–45 CrossRef Medline
29. Weller M, Felsberg J, Hartmann C, et al. **Molecular predictors of progression-free and overall survival in patients with newly diagnosed glioblastoma: a prospective translational study of the German Glioma Network.** *J Clin Oncol* 2009;27:5743–50 CrossRef Medline
30. Gunjur A, Lau E, Taouk Y, et al. **Early post-treatment pseudo-progression amongst glioblastoma multiforme patients treated with radiotherapy and temozolomide: a retrospective analysis.** *J Med Imaging Radiat Oncol* 2011;55:603–10 CrossRef Medline
31. Balana C, Capellades J, Pineda E, et al. **Pseudoprogression as an adverse event of glioblastoma therapy.** *Cancer Med* 2017;6:2858–66 CrossRef Medline
32. Ballman KV, Buckner JC, Brown PD, et al. **The relationship between six-month progression-free survival and 12-month overall survival end points for Phase II trials in patients with glioblastoma multiforme.** *Neuro Oncol* 2007;9:29–38 CrossRef Medline